Nuclear Instruments and Methods in Physics Research A 595 (2008) 631–636

Contents lists available at ScienceDirect

Nuclear Instruments and Methods in Physics Research A

journal homepage: www.elsevier.com/locate/nima

The reflection of very cold neutrons from diamond powder nanoparticles

V.V. Nesvizhevsky [a,*], E.V. Lychagin [b], A.Yu. Muzychka [b], A.V. Strelkov [b], G. Pignol [c], K.V. Protasov [c]

[a] Institute Laue-Langevin, 6 rue Jules Horowitz, F-38042 Grenoble, France
[b] Joint Institute for Nuclear Research, 141980 Dubna, Russia
[c] LPSC, UJF-CNRS/IN2P3-INPG, 53 rue des Martyrs, F-38026 Grenoble, France

ARTICLE INFO

Article history:
Received 7 May 2008
Received in revised form
16 July 2008
Accepted 22 July 2008
Available online 12 August 2008

Keywords:
Very cold neutrons
Neutron reflectors
Nanostructured materials

ABSTRACT

We study the possibility of efficiently reflecting very cold neutrons (VCN) from powders of nanoparticles. In particular, we measured the scattering of VCN on powders of diamond nanoparticles as a function of powder sample thickness, neutron velocity and scattering angle. We observed extremely intense scattering of VCN even off thin powder samples. This agrees qualitatively with the model of independent nanoparticles at rest. We show that this intense scattering would allow us to use nanoparticle powders very efficiently as the very first reflectors for neutrons with energies within a complete VCN range up to 10^{-4} eV.

1. Introduction

In the present article, we report on the feasibility of efficiently reflecting very cold neutrons (VCN) on powders of diamond nanoparticles, thus bridging the energy gap between efficient reactor reflectors [1] for thermal and cold neutrons and the effective Fermi potential for ultracold neutrons (UCN) [2–4].

The use of nanoparticles provides a sufficiently large cross-section of coherent interaction and inhomogeneity of the moderator density on a spatial scale approximately the neutron wavelength [5]. Nevertheless, a large number of neutron–nanoparticle collisions are needed for VCN reflection as they scatter in forward direction preferably. This requirement constrains the choice of materials: only low absorbing materials with high effective Fermi potential are appropriate. Diamond nanoparticles are an obvious choice as VCN reflector.

The formation of diamond particles by explosive shock was first observed more than 40 years ago [6]. Since then very intensive studies of their production and various applications have been performed worldwide. These particles measure a few nanometers [7]. Nanoparticles consist of a diamond nucleus within an onion-like shell of a complex chemical composition [8]. A recent review of the synthesis, structure, properties and applications of diamond nanoparticles can be found in Ref. [9].

One might also exploit the phenomenon of scattering off nanoparticles to study the dynamics of nanoparticles at a surface and in the material bulk [10–12]. It might also even be used to cool VCN down to the UCN energy range [13–15]. On the other hand, other studies have shown that the quasi-elastic scattering of UCN at nanoparticles on solid surfaces could be responsible for the false effects in storage experiments in fundamental particle physics [16–20].

The first experiments on the reflection of VCN from nanostructured materials as well as on VCN storage were carried out in the seventies in Ref. [21] and were later continued in Ref. [22]. We have extended the energy range and the efficiency of VCN reflection by exploiting diamond nanoparticles. A reflector of this type would be particularly useful for both UCN sources using ultracold nanoparticles [5,23] and for VCN sources; it would not be efficient however for cold and thermal neutrons, as shown in Ref. [24]. We estimated the maximum energy of the reflected neutrons. We also explored the reliability of the theoretical predictions for the interaction of neutrons with nanoparticle powders, and we provide an overview of the phenomena relevant to the interaction.

In Section 2, we describe the experimental installation developed for these studies, and the measuring procedure. In Section 3, we describe the samples of ultradiamond powder used (so-called ultradiamond90 [7]) and the procedures for measuring the intensity and the angular distribution of the scattered neutrons. In Section 4, we analyse the results, comparing them with Monte-Carlo simulations based on a model of independent nanoparticles at rest.

2. The experimental installation

The setup is shown in Fig. 1 (viewed from above). Two boron rubber diaphragms with a thickness of 5 mm shape the neutron

* Corresponding author. Tel.: +33 476 207 795; fax: +33 476 207 777.
E-mail address: nesvizhevsky@ill.fr (V.V. Nesvizhevsky).

0168-9002/$ - see front matter © 2008 Elsevier B.V. All rights reserved.
doi:10.1016/j.nima.2008.07.149

beam; the beam axis is set in a horizontal plane. The diameter of the entrance diaphragm is 16 mm. The diameter of the exit diaphragm is 10 mm. The distance between the diaphragms is 116 cm.

The neutron velocity selector (see Fig. 2) consists of a cylinder with a length of $l = 40$ cm, and a diameter of $D = 19$ cm. Plastic plates 1 mm thick are installed along the outside surface of the cylinder; they form helical slits with a width of $d = 4.5$ mm, and the screw length of $L = 480$ cm. The cylinder rotates around its axis with the period T. Neutrons can scatter at hydrogen atoms within the material of the plates; these neutrons leave the neutron beam. The rotation period defines the velocity of the neutrons passing through the selector. Neutrons with low angular divergence and with momentum parallel to the selector axis pass through the helical selector slits; they avoid being scattered by the plates if the neutron velocity is equal to $v = L2\pi/T(1 \pm dL/2\pi Dl)$. The velocity resolution of the selector is shown in Fig. 2(a). In the other case, the velocity resolution depends on the angle between the neutron momentum and the selector axis as well as on the angular divergence in the neutron beam. In order to avoid related uncertainties, we measure time-of-flight neutron spectra at the selector exit for different selector rotation periods. The average neutron velocity was measured as a function of the selector period (shown in Fig. 3(a)).

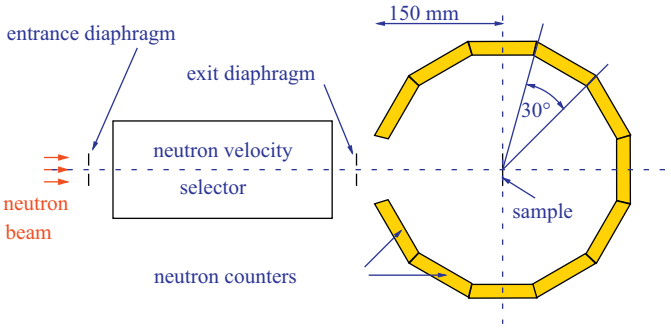

Fig. 1. The experimental setup (view from above).

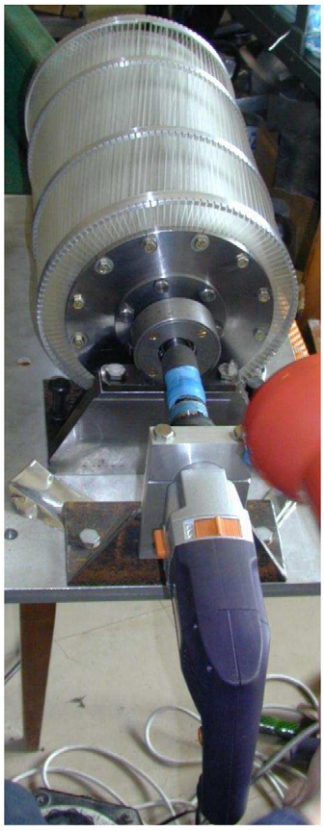

Fig. 2. The neutron velocity selector.

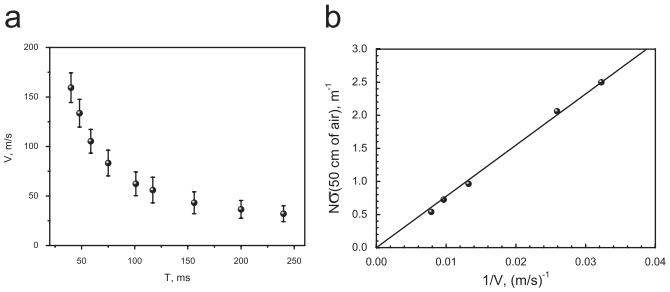

Fig. 3. (a) The average neutron velocity at the selector exit is shown as a function of the selector period. The error bars correspond to the velocity band selected. (b) The check for the $1/v$ dependance for the absorption cross-section in air.

The cross-section of neutron losses in air as a function of the neutron velocity, calibrated in such a way, agrees well with the known $1/v$ dependence (see Fig. 3b).

A sample is placed at a distance of 23 cm downstream of the exit diaphragm in the middle of the detector assembly. The detector assembly consists of 11 neutron counters measuring the neutrons scattered by the sample. The counters' flat entrance windows with the size of 17 cm × 8 cm form 11 sides of a regular 12-sided prism. The distance between sample and counter is equal to 15 cm. The total solid angle covered by the counter assembly is ≈ 45%. The neutron beam enters through the remaining 12th side which is open and perpendicular to the assembly. The counter opposite the entrance measures the neutrons passing through; its window is covered by a cadmium plate of thickness 0.5 mm. It is pierced with a 3 cm-diameter hole in the line of the beam. The other counters measure the neutrons scattered 30° in a horizontal plane and 60° in a vertical plane (the solid angle of $\pi/6$). The detector assembly is surrounded by cadmium, borated polyethylene and boron rubber neutron shielding. In order to decrease neutron scattering in the air we placed the detector assembly in a polyethylene bag filled with argon (Ar). The neutron entry window consisted of a flat quartz plate with a thickness of 3.5 mm.

Each of the 11 proportional gaseous neutron counters has a thin aluminum window with a thickness of 200 μm. The counters are filled with a mixture of Ar and ^{3}He gas at a pressure of 1 bar. The ^{3}He partial pressure is equal to 130 ± 2 mbar. The thickness of the gas-sensitive layer is 18 mm. The detection efficiency for neutrons with a velocity of 100 m/s is therefore equal to ≈ 50%; the efficiency for neutrons with a velocity of 40 m/s is equal to ≈ 85%. It should be noted that absolute efficiency values are irrelevant when measuring neutron elastic scattering probabilities if all the counters are equally efficient. Counters efficiency was calibrated using a stable neutron beam. It was equivalent for all counters within 5% precision.

3. The experiment with diamond powder nanoparticles

The measurement was carried out at the VCN PF2 beam position [25] in the Institut Laue–Langevin (Grenoble, France), providing access to neutrons with a velocity in the range of 30–160 m/s. Our sample was a powder of diamond nanoparticles

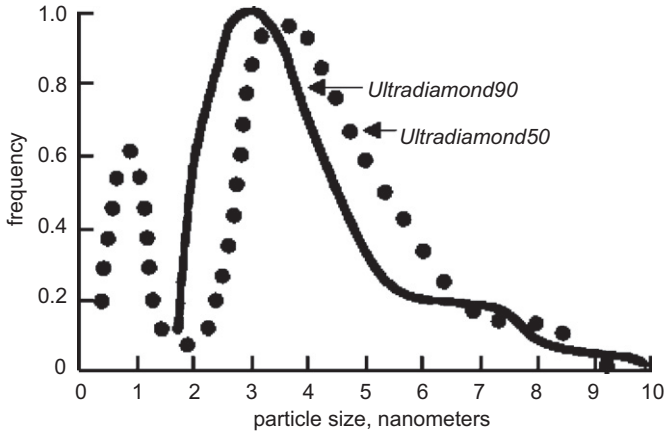

Fig. 4. The size distribution of the diamond nanoparticles in the powder "ultradiamond90".

(ultradiamond90 [7]) with diameters in the range of 2–5 nm and a known size distribution (see Fig. 4).

The powder was placed between two sapphire plates with a thickness of 1 mm each; the space between the plates was sealed on all sides with aluminum or Teflon foil. Once the powder was in position it was subjected to vibration to increase its density; the resulting density was measured by comparing the sample weight and volume. It is equal to $0.60 \pm 0.03\,\mathrm{g/cm^3}$. We prepared four samples with a thickness of 0.2, 0.4, 2 and 6 mm. The choice of thicknesses was determined as follows: the thinner the sample, the lower the multiple scattering effect. Thinner samples thus allow us to study neutron–nanoparticle interactions. The thicker the sample, the larger the reflectivity. Thicker samples thus allow us to assess the feasibility of using nanopowder as reflectors. The minimal thickness of a layer of this type, without significant holes, is 0.2 mm.

Fig. 5 presents examples of the angular dependencies measured for neutrons scattered at a 2-mm-thick sample of ultradiamond90. Any possible left–right asymmetry of the scattering probability is defined by the asymmetry in the sample plane installation. The associated systematical error is largely suppressed when averaging over symmetrical counters, as was the case in analysis.

In order to check the elasticity of the neutron scattering at the ultradiamond90 powder samples, we measured the time-of-flight spectrum of the scattered neutrons using a counter placed at an angle 150°. The average initial neutron velocity was equal to 60 m/s. In order to measure the velocity transfer at a sample we installed a chopper between the selector and the exit diaphragm. The distance between the chopper and a sample was equal to 37 cm. The time interval with the chopper open was equal to 0.5 ms. The scattering angle of 150° was chosen as the most sensitive to the neutron velocity transfer. The results of a comparison of the spectrum of scattered neutrons with the initial spectrum measured in analogous fashion are presented in Fig. 6. They show that the total average velocity change at which neutron scattering at the sample does not exceed ± 1 m/s. To demonstrate the sensitivity of this method, we also measured the scattering of neutrons at a polyethylene sample with a thickness of 2 mm. We were thus able to show that VCN scattering at the nanoparticles is mainly elastic.

4. Analysis

In order to analyse the data measured we developed a Monte-Carlo model of the experiment. The interaction of the neutrons with a nanoparticle powder can be described using the simple approach proposed in Ref. [23]. We will now outline the main features.

We neglected the relatively complex internal structure of the nanoparticle, choosing to modulate it as a uniform sphere. The neutron–nanoparticle elementary interaction was calculated using the first Born approximation. The amplitude for a neutron with energy $\hbar^2/2mk^2$ to be scattered at a spherical nanoparticle with radius R and Fermi potential V, at an angle θ is equal to

$$f(\theta) = -\frac{2m}{\hbar^2} VR^3 \left(\frac{\sin(qR)}{(qR)^3} - \frac{\cos(qR)}{(qR)^2} \right) \tag{1}$$

where $q = 2k\sin(\theta)$ is the transferred momentum. The total elastic cross-section is therefore equal to

$$\sigma_s = \int |f|^2 \, \mathrm{d}\Omega = 2\pi \left| \frac{2m}{\hbar^2} V \right|^2 R^6 \frac{1}{(kR)^2} I(kR) \tag{2}$$

where

$$I(kR) = \frac{1}{4} \left(1 - \frac{1}{(2kR)^2} + \frac{\sin(4kR)}{(2kR)^3} - \frac{\sin^2(2kR)}{(2kR)^4} \right). \tag{3}$$

The chemical composition of the nanoparticle is complex; it includes carbon (up to 88% of the total mass), hydrogen (1.0%), nitrogen (2.5%), oxygen (up to 10%) [26]. Moreover, there is a certain amount of water covering a significant surface area of the nanoparticles. In general, the hydrogen in the water and on the surface of the nanoparticles scatters the neutrons up to the thermal energy range ("up-scattering"); thermal neutrons do not interact as efficiently with nanoparticles and therefore traverse the powder. As the amount of hydrogen was not precisely known, we considered it as a free parameter in the model.

We built a Monte-Carlo model of the experiment on this basis, taking into account the sample and installation geometry described above. The size distribution of the nanoparticles in the powder is given in Fig. 4.

The simulation results are compared to the probabilities measured for forward and backward scattering of VCN at samples of all measured thicknesses as shown in Fig. 7. The two sets of curves correspond to the calculation with pure carbon nanoparticles (dotted lines) and to that with 1% of hydrogen added (solid lines). In the simulation, hydrogen is assumed to be uniformly distributed in the sample, the cross-section for (isotropic) upscattering follows the $1/v$ law, and the neutrons are assumed to escape from the sample as soon as they are upscattered. The relative efficiency of the counters for upscattered neutrons is taken to be 0.5, independent of the final velocity. The statistical accuracy of the data points is typically within their graphical size. The statistical accuracy of the Monte-Carlo simulation can be estimated using the non-smooth behaviour of the solid and dotted lines. The difference between the experimental results and the model calculation can be considered as a indication of the degree of validity of the model.

In the broad range of VCN velocities and sample thicknesses, good qualitative agreement was obtained between the probability and the angular distribution of scattered neutrons, and the predictions of the model of independent nanoparticles at rest.

In particular, the probability of the reflection of the VCN with the smallest velocities is in agreement with $\approx 100\%$ diffuse reflection, given the value of the solid angle from the sample to the counter assembly. Other neutrons are scattered to directions not covered by the counters.

The hydrogen in the powder limits the penetration of neutrons across the samples more strongly than it decreases their

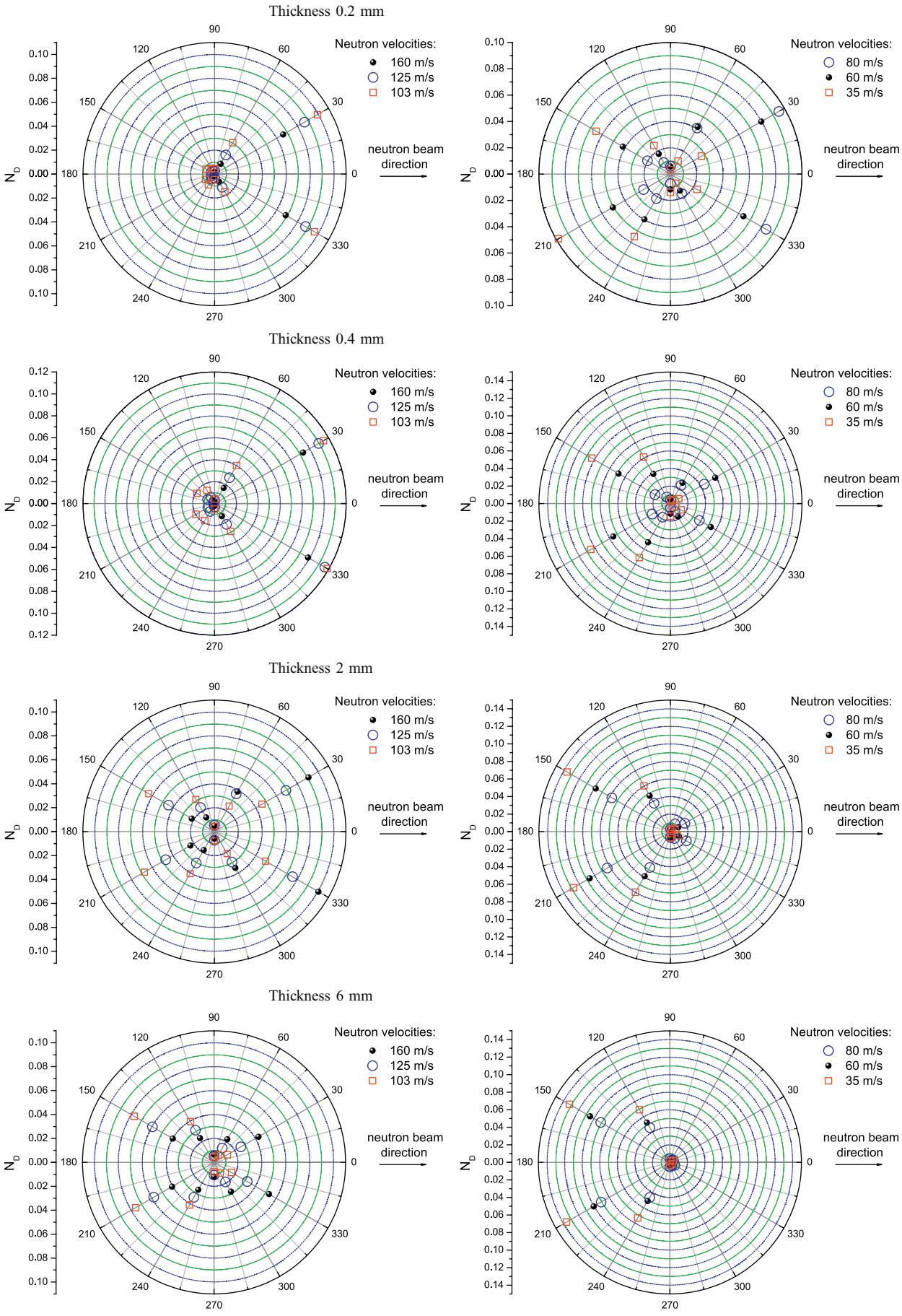

Fig. 5. The scattered neutron flux (normalized to the initial neutron flux measured in the forward counter with empty sample) is shown as a function of the scattering angle for an ultradiamond90 powder sample with a thickness of 0.2, 0.4, 2 and 6 mm. The angle measured is that between the incoming beam of neutrons and its line of flight from the sample to the centre of a corresponding counter. The results for all measured velocities from 35 to 160 m/s are indicated by the different types of point.

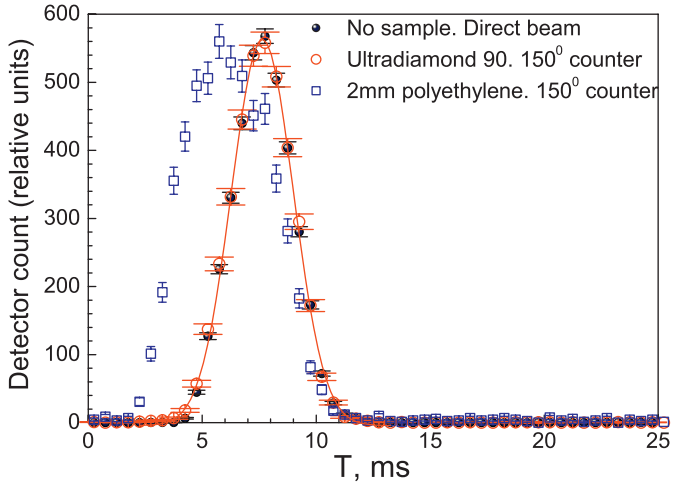

Fig. 6. The neutron count rate is presented as a function of the time of flight of the neutrons with an average initial velocity of 60 m/s. The zero time is synchronized with opening the chopper. The black circles correspond to the initial neutron spectrum. The empty circles indicate the data for the spectrum of neutrons scattered to an angle of 150°. The thickness of the ultradiamond90 powder sample is equal to 2 mm. The squares show results for the scattering of neutrons at a polyethylene sample with a thickness of 2 mm, measured at the same counter.

reflection; this effect is more pronounced for small neutron velocities and for thick samples. In future studies, we will remove the water and other hydrogen-containing impurities from the samples and will cool the powder down to liquid nitrogen temperature (at which the upscattering of neutrons at hydrogen is largely suppressed). The residual discrepancy is probably due to poor knowledge of the spatial density distribution in the powder; this variation and even holes in the samples could affect the measurements (for the thinnest samples in particular).

The present analysis could be considered as a first quality proof of the simple theoretical model presented. It will be followed by more detailed and precise studies. In particular, we should take into account the nanoparticle's geometrical shape, the distribution of the Fermi potential profile inside nanoparticles, the correlation function of their relative position, and the distribution of impurities at the nanoparticle surface. However, these more subtle effects will be studied once we have after eliminated the dominant effect of hydrogen contamination.

As can be seen from Fig. 4, the maximum energy of the reflected VCN and the reflection probability far exceed the corresponding values for the best supermirrors available [27], although the reflection is not specular at the nanopowder reflector of cause.

If the reflection of the neutrons from the ultradiamond90 powder is determined uniquely by their scattering at the nanoparticles, and if we eliminate any additional losses (due in particular to hydrogen-containing impurities), the reflection probability could be as high as is shown in Fig. 8. Efficient reflection would enable VCN to be stored in closed traps. We intend to explore this exciting hypothesis experimentally.

5. Conclusion

We observed extremely intense scattering of VCN on diamond powder nanoparticles for the first time. We demonstrated that

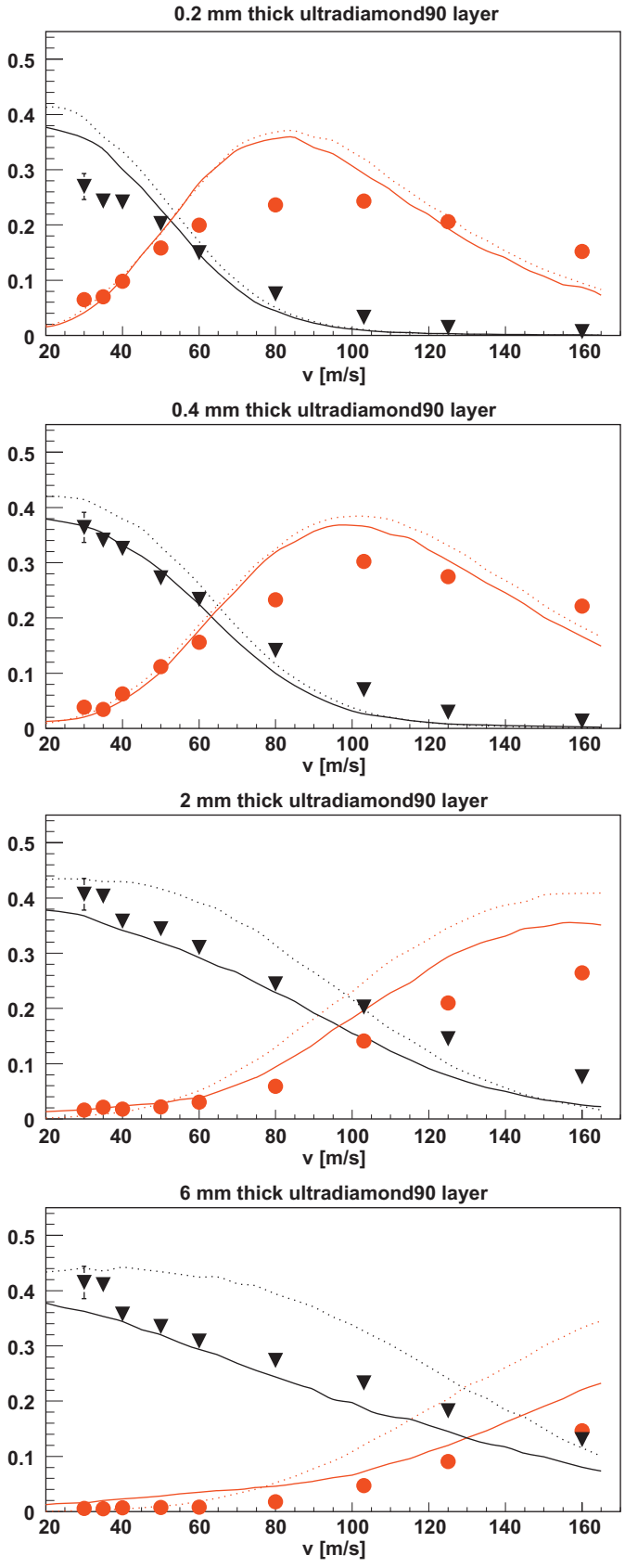

Fig. 7. The detection probability dependencies for backward (counters at $120^\circ + 150^\circ + 210^\circ + 240^\circ$) and forward (counters at $30^\circ + 60^\circ + 300^\circ + 330^\circ$) scattering of VCN at the ultradiamond90 powder are shown as a function of VCN velocity, for different powder thicknesses. The triangles correspond to the measured probability of VCN backward scattering. The circles indicate the measured probability of VCN forward scattering. The dotted lines correspond to the model of independent nanoparticles at rest. The solid lines indicate the model that takes into account the up-scattering of VCN at water in the powder.

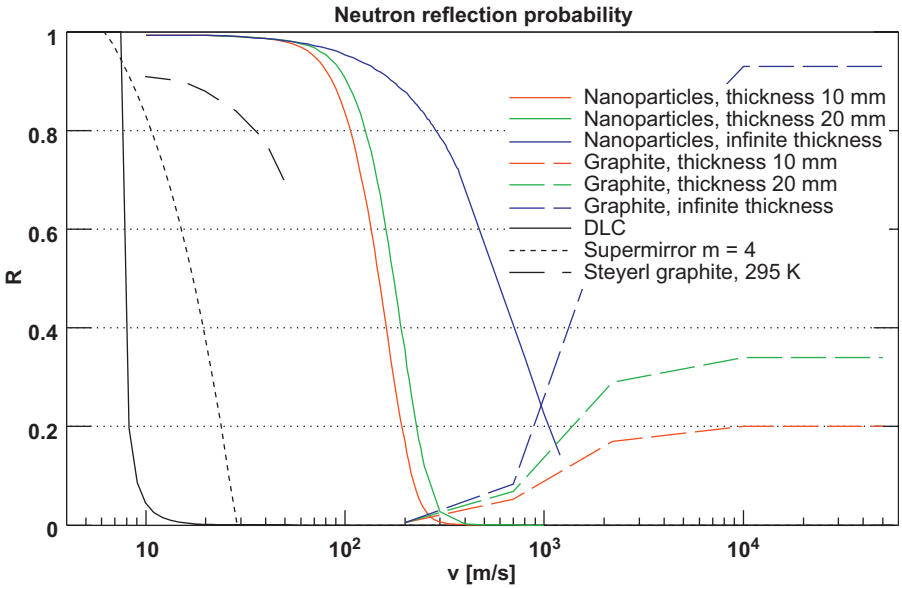

Fig. 8. The total neutron reflection probability (to all backward angles) is shown as a function of neutron velocity for various carbon-based reflectors: (1) diamond-like coating (DLC), with the highest known value of Fermi-potential (thick solid line); (2) the best supermirrors currently available [27] (dotted line); (3) Steyerl's measurement of VCN reflection [21] (dashed-dotted line); (4) hydrogen-free ultradiamond90 powder for thicknesses of 10, 20 mm, and infinite (solid lines); (5) reactor graphite reflectors at room temperature for thicknesses of 10, 20 mm, and infinite (dashed lines).

nanoparticle powders can be efficient reflectors of VCN with an energy value as high as 10^{-4} eV. This energy value and the reflection probability far exceed values for the best available supermirrors, although the reflection at nanoparticles is not specular. This phenomenon has a number of applications, including the storage of VCN in closed traps, as reflectors for VCN and UCN sources, the more efficient guiding of VCN and, probably, of even faster neutrons.

Acknowledgements

We are grateful to Y. Calzavara, P. Geltenbort and C. Plonka for their assistance. This work is supported by RFBR Grant no. 03-02-16784-a.

References

[1] E. Fermi, A course in neutron physics, in: Collected Papers, The University of Chicago Press, Chicago, 1965.
[2] R. Golub, D. Richardson, S.K. Lamoreaux, Ultra-Cold Neutrons, Adam Higler, 1991.
[3] V.K. Ignatovich, The Physics of Ultracold Neutrons, Oxford University Press, Oxford, 1990.
[4] V.I. Luschikov, Yu.N. Pokotilovsky, A.V. Strelkov, F.L. Shapiro, JETP Lett. 9 (1) (1969) 23–26.
[5] V.V. Nesvizhevsky, Phys. At. Nucl. 65 (2002) 400.
[6] P.J. De Carli, J.C. Jamieson, Science 133 (1961) 1821.
[7] ⟨http://www.ultradiamondtech.com⟩.
[8] A.E. Aleksenskii, M.V. Baidakova, A.Y. Vul', V.I. Siklitskii, Phys. Solid State 41 (1999) 668.
[9] V.Yu. Dolmatov, Russ. Chem. Rev. 76 (2007) 339.
[10] E.V. Lychagin, et al., Phys. At. Nucl. 65 (2002) 1995.
[11] D.G. Kartashov, et al., Int. J. Nanoscience 6 (6) (2007) 501.
[12] V.V. Nesvizhevsky, Phys. Usp. 46 (2003) 93.
[13] L.P. Mezhov-Deglin, V.V. Nesvizhevsky, A.V. Stepanov, Phys. Usp. 46 (2003) 89.
[14] L.P. Mezhov-Deglin, et al., J. Low Temp. Phys. 148 (2007) 833.
[15] L.P. Mezhov-Deglin, et al., J. Low Temp. Phys. 150 (3–4) (2007) 206.
[16] V.V. Nesvizhevsky, A.V. Strelkov, P. Geltenbort, P.S. Iaydjiev, Eur. J. Appl. Phys. 6 (1999) 151.
[17] V.V. Nesvizhevsky, A.V. Strelkov, P. Geltenbort, P.S. Iaydjiev, Phys. At. Nucl. 62 (1999) 776.
[18] A.V. Strelkov, et al., Nucl. Instr. and Meth. A 440 (2000) 695.
[19] E.V. Lychagin, et al., Phys. At. Nucl. 63 (2000) 548.
[20] V.V. Nesvizhevsky, et al., Phys. Lett. B 479 (2000) 353.
[21] A. Steyerl, W.-D. Trüstedt, Z. Physik 267 (1974) 379.
[22] S.S. Arzumanov, et al., Phys. At. Nucl. 68 (2005) 1141.
[23] V.V. Nesvizhevsky, G. Pignol, K.V. Protasov, Int. J. Nanoscience 6 (6) (2007) 485.
[24] V.A. Artem'ev, At. Energy 101 (2006) 901.
[25] ⟨http://www.ill.fr/YellowBook/PF2⟩.
[26] A.L. Vereschagin, G.V. Sakovich, V.F. Komarov, E.A. Petrov, Diamond Relat. Mater. 3 (1993) 160.
[27] R. Maruyama, et al., Thin Solid Films 515 (2007) 5704.